



Synthesis, structure and characterisation of *rac* and *meso*-ansa-bridged permethylindenyl cobalt complexes

Paul Ransom, Andrew Ashley, Amber Thompson, Dermot O'Hare *

Chemistry Research Laboratory, Department of Chemistry, University of Oxford, Mansfield Road, Oxford OX1 3TA, UK

ARTICLE INFO

Article history:

Received 21 July 2008

Received in revised form 27 August 2008

Accepted 2 September 2008

Available online 10 September 2008

Dedicated to Professor Dr. Ch. Elschenbroich on the occasion of his 70th birthday.

Keywords:

ansa-Metallocenes

Cobaltocenes

Metallocenes

Indenyl

ABSTRACT

Disodium ethylene-bis-hexamethylindenyl, $\{(C_9Me_6)_2C_2H_4\}Na_2$ (EBI^*Na_2), has been prepared in good yield by the reaction of lithium heptamethylindenyl with cyanogen bromide followed by treatment with sodium naphthalenide. EBI^*Na_2 reacts with anhydrous $Co(acac)_2$ to give a mixture of *rac* and *meso*-ethylene-bis-hexamethylindenyl cobalt(II) (EBI^*Co). The isomers can be separated by fractional crystallisation and the *rac*-isomer has been structurally characterised. Oxidation of the reaction mixture yields both *rac* and *meso*-ethylene-bis-hexamethylindenyl cobalt(III) which have both been structurally characterised.

© 2008 Elsevier B.V. All rights reserved.

1. Introduction

The cyclopentadienyl ligand (Cp) is ubiquitous in organometallic chemistry, and can be modified in a myriad of ways. One such modification is the introduction of a linking group between the two Cp rings of metallocenes to form *ansa*-metallocenes. The Latin prefix *ansa* means bent handle attached at both ends, and various atoms or groups can make up the bridge, including C, Si, and heteroatom moieties [1]. Numerous *ansa*-metallocenes of the early transition metals, main group and lanthanides are known, their reactivity compared to their unbridged analogues being affected; either enhanced retarded or completely altered [1,2]. The *ansa* bridge also has an effect on structure, the distortion and strain present dependent on how many atoms long the bridge is and what atoms or groups make up the bridge.

Strained ferrocenophanes such as $\{(C_5H_3R)_2C_2H_4\}Fe$ (R = H, Me) undergo ring-opening polymerisation (ROP) to yield high molecular weight polymers; the use of different spacer groups, metals and π hydrocarbon ligands allows the properties of the metallopolymer to be tuned for specific applications [3,4]. However, in order for the polymers produced to be soluble in organic solvents, the Cp ring must be methylated. Despite the large amount of work that has been performed on strained ferrocenophanes, the area of strained cobaltocenophanes is virtually undeveloped, yet interesting due to the high degree of interaction between Co centres that is

expected to be much greater than that between Fe centres in poly-metallocenes [5]. ROP on neutral 19-electron cobaltocenophanes may produce polymers with interesting electronic properties, due to electronic coupling between adjacent paramagnetic Co centres. However, there are only two examples reported of neutral hydrocarbon-bridged cobaltocenophanes, both with unsubstituted Cp ring moieties [6]. Furthermore, ROP on oxidised 18-electron Co(III) derivatives may be expected due to their isoelectronic relationship with ferrocenophanes. The charged polycobaltocenes produced should show increased solubility in polar solvents, in contrast with non-functionalised uncharged polyferrocenes.

This article details the synthesis and characterisation of a new *ansa*-bridged ligand species ethylene-bis-hexamethylindenyl (EBI^*), $\{(C_9Me_6)_2C_2H_4\}^{2-}$, and its utilisation in the synthesis of a strained paramagnetic 19-valence electron Co species. This is the first example of a hydrocarbon-bridged cobaltocenophane with permethylated ring systems. Furthermore, the ethylidene bridge is sterically non-demanding, beneficial when considering the susceptibility of the monomer to ROP. The ligand synthesis by reductive dimerisation of the fulvene $C_{16}H_{20}$ yields the EBI^* moiety containing an unsubstituted ethyl bridge, in contrast with reports requiring substitution of the 6-position in fulvenes in order to stabilise the intermediate radical anion sufficiently to dimerise [7,8]. This stabilisation is facilitated via the delocalisation of the negative charge of the radical anion obtained after the metal mediated reduction over the aryl ring of the indenyl moiety. The oxidation of the neutral Co(II) species is also described and the diamagnetic air-stable 18-valence electron products characterised.

* Corresponding author. Tel.: +44 1865 285130; fax: +44 1865 285131.

E-mail address: dermot.ohare@chem.ox.ac.uk (D. O'Hare).

2. Results and discussion

2.1. Synthesis and characterisation of disodium ethylene-bis-hexamethylindenyl, $\text{EBI}^* \text{Na}_2$ (**1**)

Disodium ethylene-bis-hexamethylindenyl, $\{(\text{C}_9\text{Me}_6)_2\text{C}_2\text{H}_4\}\text{Na}_2$ ($\text{EBI}^* \text{Na}_2$) (**1**) can be prepared in good yield by the reaction of lithium heptamethylindenyl with cyanogen bromide followed by treatment of the resulting 2,3,4,5,6,7-hexamethyl-1-methylene-indene, $\text{C}_{16}\text{H}_{20}$ with sodium naphthalenide (Fig. 1).

2,3,4,5,6,7-hexamethyl-1-methylene-indene was isolated as a bright yellow powder and characterised by ^1H and ^{13}C NMR spectroscopy, showing indicative fulvenyl proton shifts at 5.56 and 5.84 ppm, and high resolution mass spectrometry. The radical coupling of $\text{C}_{16}\text{H}_{20}$ moieties is initiated by the transfer of an electron from the radical anion $(\text{C}_{10}\text{H}_8)^-\text{Na}^+$ produced upon treatment of naphthalene with Na, affording $(\text{C}_{16}\text{H}_{20})^-\text{Na}^+$ and C_{10}H_8 . These indenyl radical anions can then couple in solution to give the dimetallated ligand precursor. This proceeds in 76% yield affording **1** as a highly air sensitive light brown powder, which was identified by ^1H and ^{13}C NMR spectroscopy.

2.2. Synthesis and characterisation of ethylene-bis-hexamethylindenyl cobalt, $\text{EBI}^* \text{Co}$ (**2**)

Ethylene-bis-hexamethylindenyl cobalt, $\text{EBI}^* \text{Co}$ (**2**) was prepared in moderate yield (51%) by the reaction of $\text{Co}(\text{acac})_2$ and **1** in THF, as shown in Fig. 2. The yield is significantly higher than the only other two syntheses of neutral, paramagnetic 19-valence electron hydrocarbon bridged cobaltocenophanes, i.e. $\{(\text{C}_5\text{H}_4)_2\text{C}_2\text{H}_4\}\text{Co}$ and $\{(\text{C}_5\text{H}_4)_2\text{C}_3\text{H}_6\}\text{Co}$ which proceed in very low yields of 9% and 8%, respectively [6].

The reaction mixture contains both *rac* and *meso*-isomers. The *rac*-isomer may be selectively crystallised by cooling a hexane solution of the isomeric mixture to -78°C . Removal of the solvent from the -78°C supernatant showed it to be a 1:1 mixture of *rac* and *meso*-isomers. *Rac-2* has been characterised by elemental analysis, high resolution mass spectrometry, and single-crystal X-ray diffraction. It is paramagnetic in solution, with only one broad resonance being observed in the ^1H NMR spectrum at 14.5 ppm in C_6D_6 in the range -100 ppm to 100 ppm.

The electrochemical behaviour of *rac-2* was studied as a $2.0 \times 10^{-3} \text{ mol L}^{-1}$ solution in THF with $0.1 \text{ mol L}^{-1} [\text{NBu}_4][\text{PF}_6]$ as supporting electrolyte. Data were recorded at room temperature at a scan rate of 100 mV s^{-1} , referenced to the $\text{Cp}_2\text{Fe}/\text{Cp}_2\text{Fe}^+$ couple at +1.36 V vs. SCE. The thermodynamic half potential for the oxidation couple $[\text{rac-2}]^{0/+}$ is +0.14 V. For comparison, the redox potentials for related cobaltocenes are as follows: Cp_2Co +0.10 V; Cp^*Co -0.46 V, and the ethylidene bridged species $\{(\text{C}_5\text{H}_4)_2\text{C}_2\text{-H}_4\}\text{Co}$ +0.06 V [6]. The redox potentials for the *ansa*-cobaltocenes *rac-2* and $\{(\text{C}_5\text{H}_4)_2\text{C}_2\text{H}_4\}\text{Co}$ are similar, the oxidation potential of *rac-2* does not appear to reduce upon methylation of the five-membered ring as may have been anticipated and as is the case with other metallocenes. This may be due to the increased ring tilt in $\{(\text{C}_5\text{H}_4)_2\text{C}_2\text{H}_4\}\text{Co}$ (see values of α in Table 5). This effect is also witnessed in the potential of the unstrained compound $(\text{C}_5\text{H}_4\text{Me})_2\text{-Co}$, which is more positive than that of the strained $\{(\text{C}_5\text{H}_4)_2\text{-C}_2\text{H}_4\}\text{Co}$.

The solid state magnetic susceptibility of *rac-2* obeys the Curie Law between 50 K and 300 K with an effective moment of $\mu_{\text{eff}} = 1.65\mu_{\text{B}}$. In solution the moment is determined by the Evans NMR method to be $1.86\mu_{\text{B}}$. These two values correspond very favourably to the expected spin-only value for one unpaired electron.

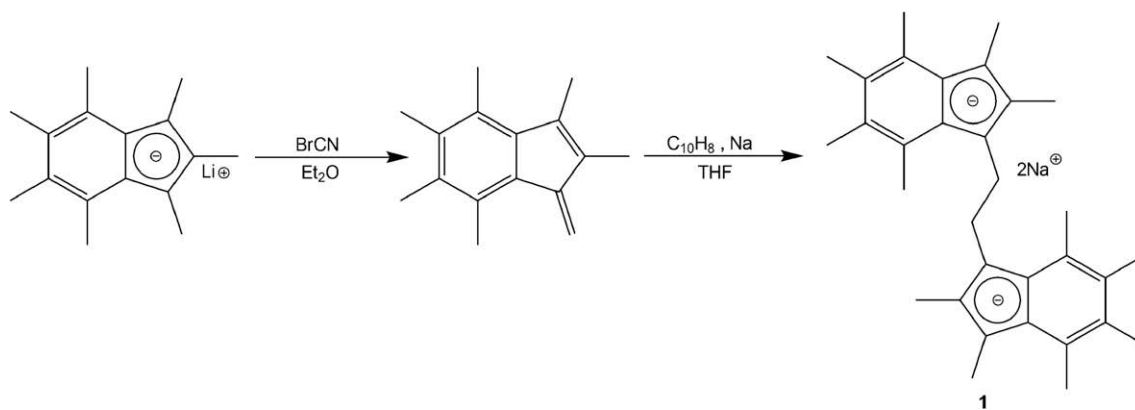


Fig. 1. Synthesis of disodium ethylene-bis-hexamethylindenyl, $\text{EBI}^* \text{Na}_2$ (**1**).

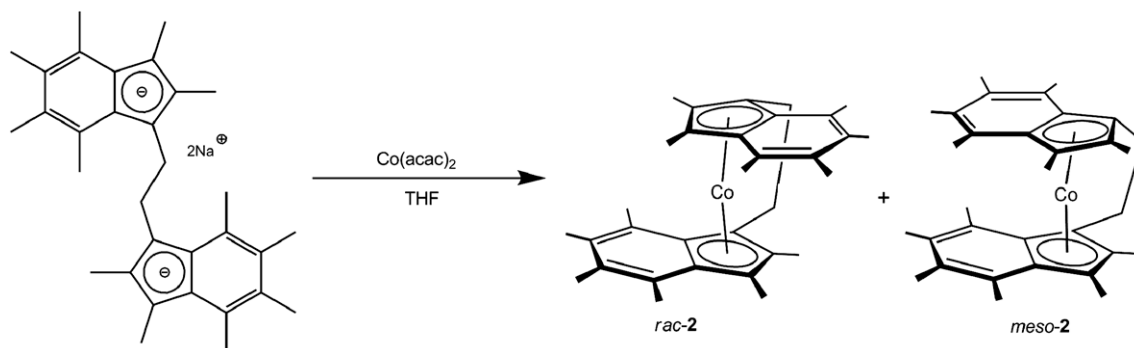


Fig. 2. Synthesis of *rac* and *meso*- $\text{EBI}^* \text{Co}$ (**2**).

2.3. Synthesis and characterisation of *rac* and *meso*-[EBI*Co]⁺X⁻, X = Cl (**3**), PF₆⁻ (**4**)

[EBI*Co]Cl (**3**) was prepared by addition of an aqueous solution of NH₄Cl in the presence of atmospheric oxygen to a solution of **2**. Extraction with CH₂Cl₂ yields an orange solid. Compound **3** has been characterised by ¹H and ¹³C NMR spectroscopy and high resolution mass spectrometry. Single crystals of [*rac*-EBI*Co]₂[CoCl₄](CH₂Cl₂)₂ (*rac*-**5** · CH₂Cl₂) suitable for single-crystal X-ray diffraction were grown by the slow diffusion of Et₂O into a concentrated CH₂Cl₂ solution of pure *rac*-**3**. Crystals of the *meso*-isomer were obtained as [*meso*-EBI*Co]₂[CoCl₄](CH₂Cl₂) (*meso*-**5**) by the slow diffusion of Et₂O into a concentrated CH₂Cl₂ solution of the 1:1 *rac*/*meso*-**3** mixture.

The formation of cobaltocenium compounds with CoCl₄²⁻ counterions has been reported in the literature. For example, the reaction of (C₅H₄^tBu)Na with [Co(NH₃)₆]Cl₂ in THF produces, after recrystallisation from CH₂Cl₂/hexane, [(C₅H₄^tBu)₂Co]₂[CoCl₄] [**9**]. In addition, the one-electron transfer process on reaction of Cp₂Co with Ph₃CCl produces [Cp₂Co]⁺, which surprisingly forms the CoCl₄ salt in dioxane/ethanol solvent mixtures. Furthermore, [Cp₂Co]₂[CoCl₄] can also be obtained directly from the reaction of Cp₂CoCl with anhydrous CoCl₂ in ethanol [**10**].

The ¹H NMR spectra of isomerically pure samples of *rac*-**5** · CH₂Cl₂ and *meso*-**5** showed resonances which were broadened and shifted compared with the parent spectra of *rac* and *meso*-**3**, respectively. This may be explained by the presence of the paramagnetic counterion [CoCl₄]²⁻, as observed in the spectrum of [Cp₂Co]₂[CoCl₄] compared with [Cp₂Co]Cl [**10**]. Interestingly, when the supernatant was decanted and the solvent removed under vacuum, analysis by ¹H NMR spectroscopy showed only compound **3**

to be present, the spectra not being paramagnetically broadened or shifted.

Conversion to [EBI*Co]PF₆ (**4**) was achieved by precipitation from an aqueous solution of **3** upon addition of a saturated aqueous solution of NH₄PF₆. ¹H and ¹³C NMR of the mixture of *rac* and *meso* salts has been completely assigned. The protons of the ethylidene bridge serve as a stereochemical probe; analysis of the AA'BB' multiplet structure allows the determination of the dihedral angles between vicinal protons. Each carbon atom of the C₂-bridge has two chemically distinct protons, H_A and H_B, and these are magnetically non-equivalent to their analogues on the neighbouring bridge-carbon. As shown in Fig. 3, in the *rac*-isomer H_A/H_{A'} and H_B/H_{B'} are on opposite sides of the bridge to one another, whereas in the *meso* form H_A/H_{A'} and H_B/H_{B'} are on the same side of the bridge. This was further confirmed by a series of nOe experiments.

In the case of the *meso*-isomer, in order to simulate the spectrum observed the rings must be either completely eclipsed or dynamic. However in the *rac* form the dihedral angle differences will be the same whether the rings are dynamic or not, allowing approximate angles to be calculated between H_A/H_{A'}, H_A/H_B and H_B/H_{B'} of 105°, 15° and 149°, respectively. The crystal structure of *rac*-**5** · CH₂Cl₂ shows similar values; 85°, 34° and 153°, respectively, compared with 31°, 150° and 30°, respectively, for the *meso*-isomer.

Fig. 4 shows the spectrum obtained in CD₂Cl₂ of the bridging protons of a 1:1 mix of *rac* and *meso*-**4**, together with the simulated spectrum using the coupling constants calculated (see Section 3.5). The multiplet of the *rac*-isomer is separated into two distinct regions, 3.58–3.67 ppm and 3.86–4.00 ppm, whereas the *meso* multiplet covers one region from 3.61–3.77 ppm. This is due to the different magnitudes of the coupling constants between protons of the bridge in the two isomers, due to their different dihedral angles relative to one another.

For completeness, the 700 MHz spectrum was also recorded and accurately simulated in a similar manner. This assignment of the spectra of the mixture of *rac* and *meso*-**4** was confirmed by running ¹H and ¹³C NMR spectra of a sample of *rac*-**4** synthesised from a sample of pure *rac*-**3** used to grow crystals of *rac*-**5** · CH₂Cl₂.

A common feature of strained hydrocarbon-bridged metallocenophanes is a downfield shift in the resonance of the *ipso*-carbon observed in the ¹³C NMR spectrum. For example, the ¹³C chemical shift for C_{ipso} in [(C₅H₄)₂C₂H₄]Co is 110.8 ppm whereas the other two carbon environments of the five-membered ring have shifts of 84.8 and 86.3 ppm [**6**]. In contrast, in *rac*-**4** C_{ipso} is detected at 96.89 ppm, and the other four carbons of the five-membered ring at 84.79, 92.94, 101.00 and 103.81 ppm. Similar shifts are also observed for the *meso*-isomer.

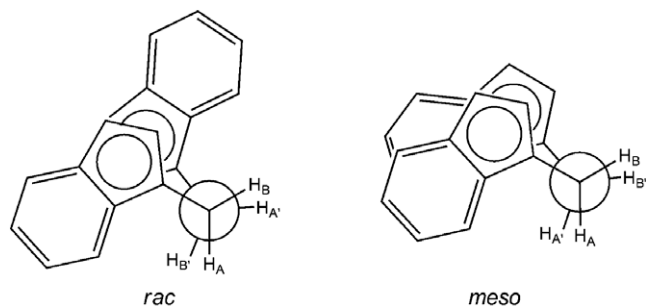


Fig. 3. Newman projection of the EBI* ligand viewed down the C₂-bridge, with methyl groups removed for clarity.

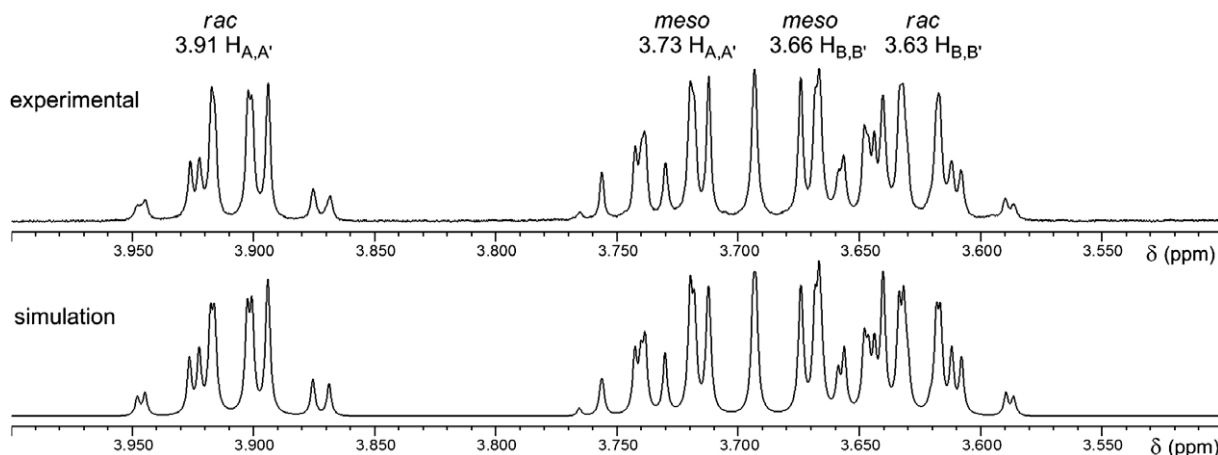


Fig. 4. 500 MHz experimental (top) and simulated (bottom) spectra in CD₂Cl₂ of the region of the ethylidene bridge protons of a 1:1 mixture of *rac* and *meso*-**4**.

2.4. Structural analysis of *rac*-2, *rac*-5 (CH_2Cl_2) and *meso*-5

Crystals of *rac*-2 suitable for single-crystal X-ray diffraction were grown as dark purple plates by the cooling of a hexane solution to $-78\text{ }^\circ\text{C}$. The compound crystallises in the monoclinic space group $C2/c$. Three alternative views are shown in Fig. 5.

As shown in Fig. 5, the indenyl group is significantly distorted from planarity. With respect to the best plane of the six-membered ring, C(1) is displaced by 0.15 \AA towards the ring junction whereas C(2) and C(3) are displaced by 0.09 \AA away. The five-membered ring can be seen to have a shallow envelope conformation such that the angle between the best planes of the fragments C(5), C(1), C(2) and C(2), C(3), C(4), C(5) is 11.0° . The complex is located on a crystallographic twofold axis of rotation, both indenyl rings being equivalent. Relevant bond distances are given in Table 1.

Attempts to grow single crystals of *rac*-3 by the slow diffusion of Et_2O into a CH_2Cl_2 solution resulted in orange-brown prisms, of the formula $[\text{rac-EBI}^*\text{Co}]_2[\text{CoCl}_4](\text{CH}_2\text{Cl}_2)_2$, (*rac*-5 $\cdot \text{CH}_2\text{Cl}_2$). The compound crystallises in the monoclinic space group $P2_1$, and three alternative views are shown in Fig. 6.

The asymmetric unit contains two *rac*-[EBI * Co] $^+$ moieties, one of each enantiomer, together with one $[\text{CoCl}_4]^{2-}$ counterion and two molecules of CH_2Cl_2 . The structure seems to exhibit a lot of thermal motion in the indenyl moieties, however this does not change the connectivity and the prolate ellipses describe the dynamics very clearly. The other enantiomer, not shown in Fig. 6, also shows this thermal motion, however to a lesser extent. Unlike *rac*-EBI * Co, each enantiomer in the asymmetric unit does not lie on a C_2 -axis, hence each indenyl ring is independent and so bond lengths shown in Table 2 have been chosen for one of the four indenyl moieties in the asymmetric unit.

Analogous to the *rac*-isomer, attempts to grow single crystals of *meso*-3 by the slow diffusion of Et_2O into a CH_2Cl_2 solution of a 1:1 mixture of *rac* and *meso*-3 resulted in orange-brown prisms, of the

Table 1
Selected bond lengths in *rac*-2

Bond	Length (Å)	Bond	Length (Å)
Co(1)–C(1)	1.9860(18)	C(3)–C(4)	1.457(3)
Co(1)–C(2)	2.0593(18)	C(4)–C(5)	1.442(3)
Co(1)–C(3)	2.0879(18)	C(9)–C(4)	1.425(3)
Co(1)–C(4)	2.1708(18)	C(5)–C(6)	1.421(3)
Co(1)–C(5)	2.1933(18)	C(6)–C(7)	1.392(3)
C(1)–C(2)	1.441(3)	C(7)–C(8)	1.429(3)
C(1)–C(5)	1.466(3)	C(8)–C(9)	1.387(3)
C(2)–C(3)	1.429(3)	C(3)–C(4)	1.457(3)

ESDs are given in parentheses.

formula $[\text{meso-EBI}^*\text{Co}]_2[\text{CoCl}_4](\text{CH}_2\text{Cl}_2)$ (*meso*-5). The compound crystallises in the monoclinic space group $C2/c$, and three alternative views are shown in Fig. 7.

In the *meso* form, the asymmetric unit contains one $[\text{EBI}^*\text{Co}]^+$ moiety, with half an equivalent of the counterion CoCl_4^{2-} and half a CH_2Cl_2 molecule. As for the *rac*-isomer, the geometry of both indenyl rings is slightly different; hence Table 3 shows bond lengths for only one of the two indenyl rings within the asymmetric unit.

In order to make general comparisons between the solid state structures of indenyl complexes, a number of parameters have previously been defined [11]. The rotation angle (RA) is the angle formed by the intersection of the two planes determined by the centroids of the five- and six-membered rings, as shown in Fig. 8a. A rotation angle of 0° would indicate a fully eclipsed geometry whereas an angle of 180° corresponds to a fully staggered arrangement of the rings. The slip parameter, $\Delta_{\text{M-C}}$ is defined as the difference in the average bond lengths of the metal to bridge-head carbons and the metal to the adjacent carbons of the five-membered ring, shown in Fig. 8b. A value of $\Delta_{\text{M-C}} = 0$ indicates an η^5 bonding situation, whereas a larger value indicates a move

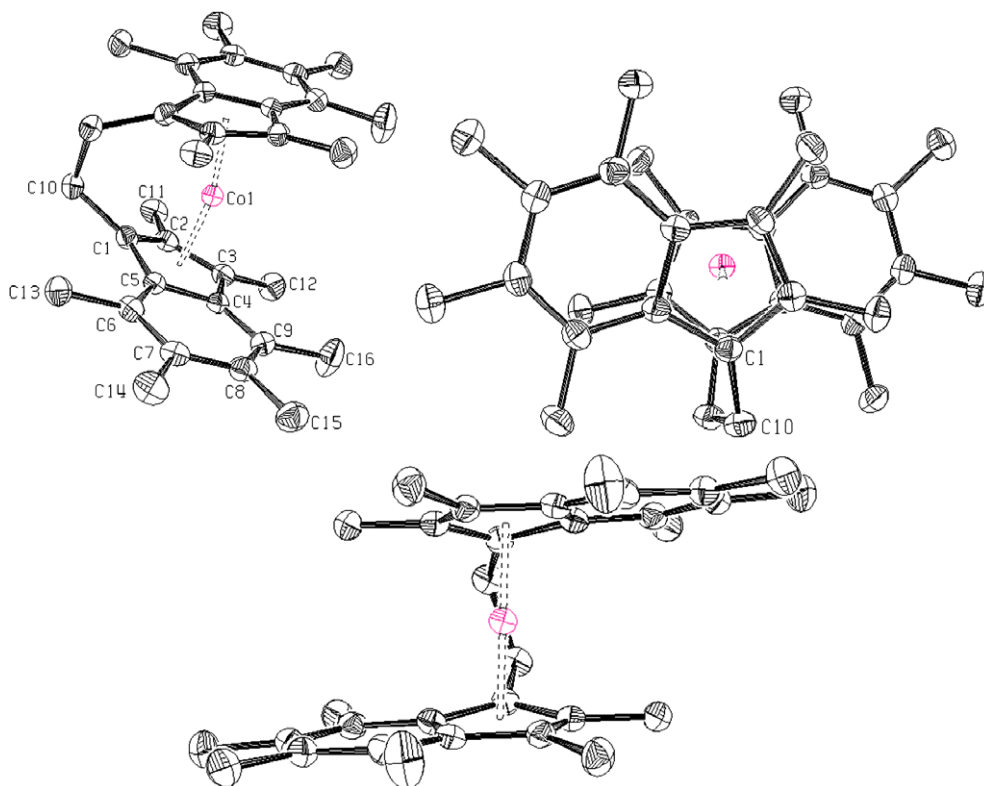


Fig. 5. Three views of *rac*-2, with hydrogen atoms omitted for clarity and thermal ellipsoids drawn at 50%.

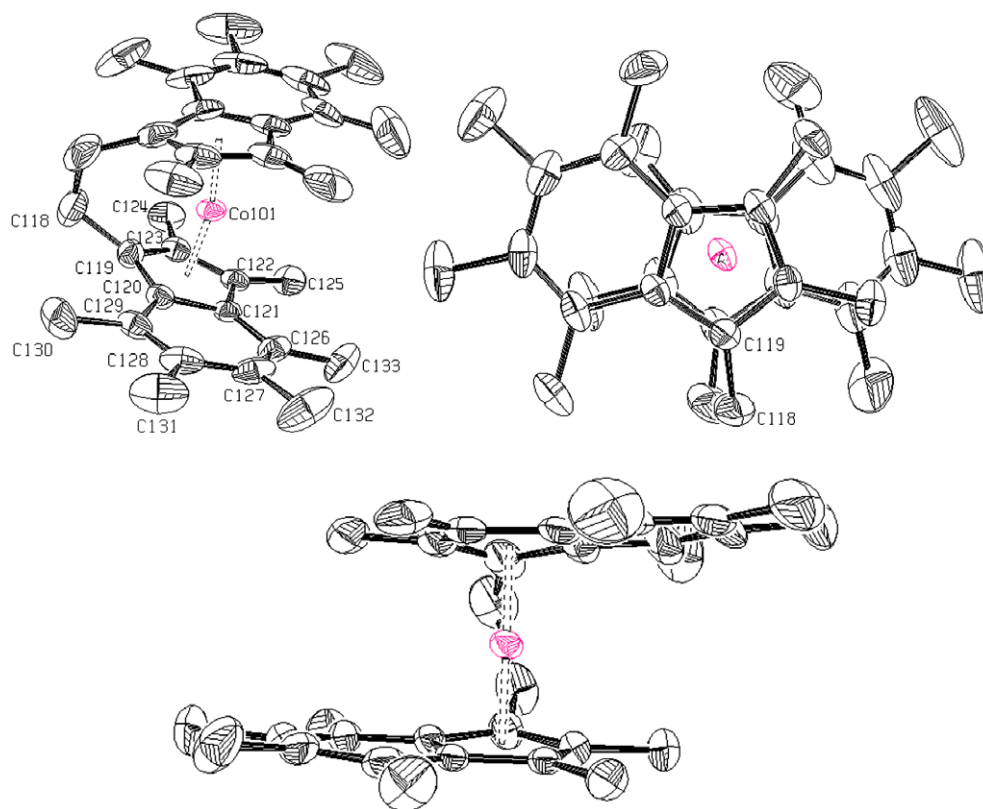


Fig. 6. Three views of one of the two $[\text{EBI}^*\text{Co}]^+$ moieties in the asymmetric unit of $\text{rac-5} \cdot \text{CH}_2\text{Cl}_2$, with hydrogen atoms, counterion and two CH_2Cl_2 molecules omitted for clarity. Thermal ellipsoids are drawn at 50%.

Table 2
Selected bond lengths in $\text{rac-5} \cdot \text{CH}_2\text{Cl}_2$

Bond	Length (Å)	Bond	Length (Å)
Co(101)–C(119)	1.978(4)	C(3)–C(4)	1.457(3)
Co(101)–C(120)	2.056(3)	C(4)–C(5)	1.442(3)
Co(101)–C(121)	2.079(3)	C(9)–C(4)	1.425(3)
Co(101)–C(122)	2.079(3)	C(5)–C(6)	1.421(3)
Co(101)–C(123)	2.079(3)	C(6)–C(7)	1.392(3)
C(119)–C(120)	1.455(5)	C(7)–C(8)	1.429(3)
C(119)–C(123)	1.444(5)	C(8)–C(9)	1.387(3)
C(120)–C(121)	1.453(5)		

ESDs are given in parentheses.

to η^{-3} coordination. The hinge angle (HA) shown in Fig. 8c, represents the degree to which the *ipso*-carbon atom is bent out of the plane of the other four carbons on the five-membered ring.

As shown in Table 4, the RA for rac-2 and the oxidised form $\text{rac-5} \cdot \text{CH}_2\text{Cl}_2$ are similar, as may be expected from the geometric restrictions of the bridging ethyl moiety holding both rings in place. The *meso*-isomer has a much lower value, with the indenyl rings being almost eclipsed. Again, this may be expected due to the restriction upon rotation of the rings with respect to one another by the ethylidene bridge.

It can also be seen in Table 4 that upon oxidation, a notable drop in the value of $\Delta_{\text{M-C}}$ occurs, indicating a move from a partially η^3 bonding situation to a more η^5 mode. This ring slip towards a η^3 mode in rac-2 may be an electronic effect, reducing the electron count at the 19-electron Co centre. Oxidation results in the Co centre obtaining an 18-valence electron count, hence a shift towards η^3 coordination is not energetically favoured and is not observed.

The ring slippage in rac-2 , and concomitant aromatisation of the aryl ring, is borne out in the carbon-carbon bond lengths within

the five- and six-membered rings, as shown in Table 1. In both $\text{rac-5} \cdot \text{CH}_2\text{Cl}_2$ and *meso-5*, bond length alternation within the aryl ring and a similarity in bond lengths within the five-membered ring is observed, shown in Tables 2 and 3. This is as would be expected, with alternating single and double bonds within the aryl ring and a delocalisation of electrons within the η^5 five-membered ring. However, in rac-2 , the extent of this alternation within the aryl ring is reduced, and instead an alternation in the five-membered ring is observed, the bonds between the ring junction carbons and the adjacent carbons of the five-membered ring being longer. This is consistent with a move to η^3 coordination and aromatisation of the aryl ring.

The HA represents bending at the carbons of the five-membered ring adjacent to the ring junction, and so can also be used as an indication of the hapticity of the bonding to the metal centre. A larger HA is associated with a distortion away from η^5 geometry, as the data in Table 4 show in the case of the neutral rac-2 , whereas both oxidised isomers have a lower HA due to the more η^3 bonding characteristics of the EBI^* ligand in these cases.

Several parameters can be used to quantify the strain present in *ansa*-bridged species and their distortion from the structure of a typical metallocene such as Cp_2Co , as shown in Table 5. In cyclopentadienyl species, the tilt angle α is defined as the angle subtended between the two planes of the five-membered rings. However, in the EBI^* moiety all five carbon atoms of the five-membered ring are not coplanar, the *ipso*-carbon being out of the plane towards the metal centre, as quantified by HA. Fig. 9 shows two angles, α and α' , the angles subtended by the average plane of the five carbons of the five-membered ring and by the plane of the four coplanar carbon atoms, respectively. Similarly, the angle β is that formed by the plane of the atoms of the five-membered ring and the vector of the *ipso*-carbon to bridge-carbon bond. Hence, Fig. 9

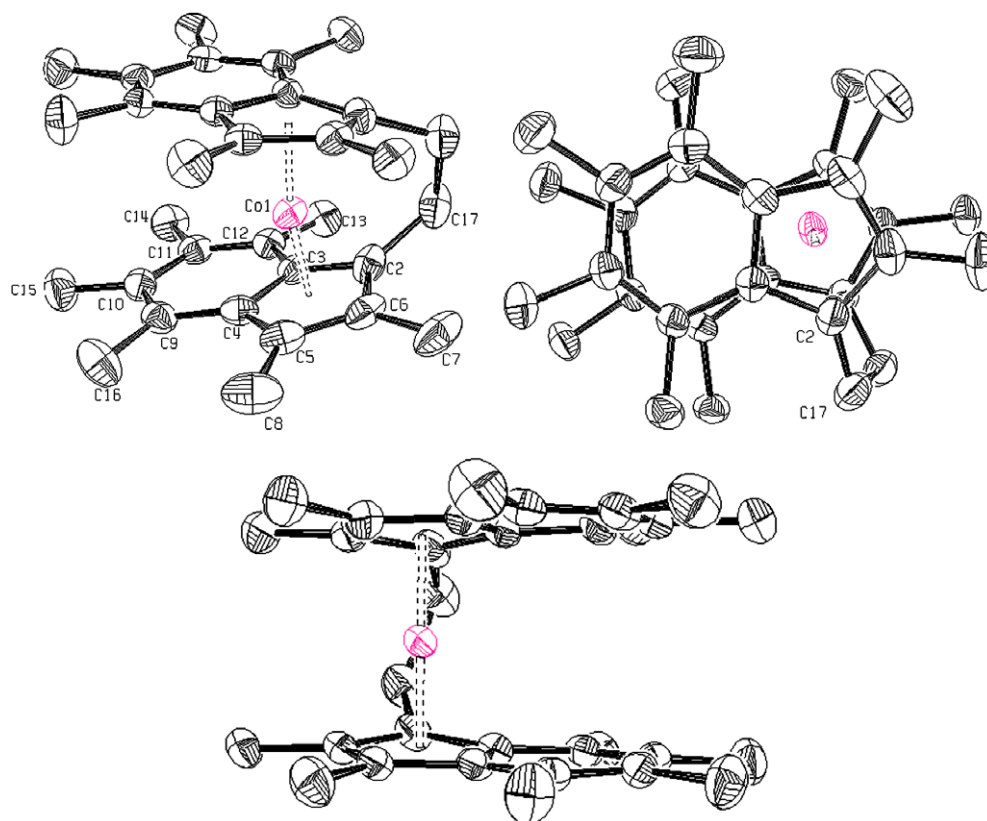


Fig. 7. Three views of *meso-5*, with hydrogen atoms and half of the counterion and CH_2Cl_2 molecule omitted for clarity. Thermal ellipsoids are drawn at 50%.

Table 3
Selected bond lengths in *meso-5*

Bond	Length (Å)	Bond	Length (Å)
Co(1)–C(2)	1.974(3)	C(3)–C(12)	1.438(4)
Co(1)–C(3)	2.076(2)	C(4)–C(5)	1.444(4)
Co(1)–C(4)	2.085(3)	C(4)–C(9)	1.432(4)
Co(1)–C(5)	2.064(3)	C(5)–C(6)	1.430(5)
Co(1)–C(6)	2.040(3)	C(9)–C(10)	1.369(4)
C(2)–C(3)	1.455(4)	C(10)–C(11)	1.448(4)
C(2)–C(6)	1.436(4)	C(11)–C(12)	1.448(4)
C(3)–C(4)	1.450(4)		

ESDs are given in parentheses.

shows angles β and β' formed in EBI^* from the plane of the five non-coplanar carbons and four planar carbon atoms of the five-membered ring, respectively (Fig. 10).

Table 5 shows a number of data of other ethylidene bridged cobalt reference species. The values of α and α' for **2** and its oxidised derivatives are lower than might be expected when compared with other related compounds. It might be anticipated that the steric repulsion between the methyl groups on opposite rings would force the rings apart and raise the value of α , however this is offset by stronger metal–carbon bonding due to the increased electron donating properties of the ligand through permethylation of the ring periphery, thus pulling the two ring planes together and reducing α . Oxidation of **2** results in a structural change with a decrease in the values of α and α' , as observed in Table 5 for $\{(\text{C}_5\text{H}_4)_2\text{C}_2\text{H}_4\}\text{Co}$. This may be explained by referral to the molecular orbitals of metallocenes, as an electron is removed from an antibonding orbital in going from a d^7 to a d^6 metal centre. This is also reflected in the shortening of the $\text{M}-\text{Cp}_{\text{centroid}}$ distance on oxidation and reduction in the angle δ , as the five-membered rings are pulled in towards the metal centre.

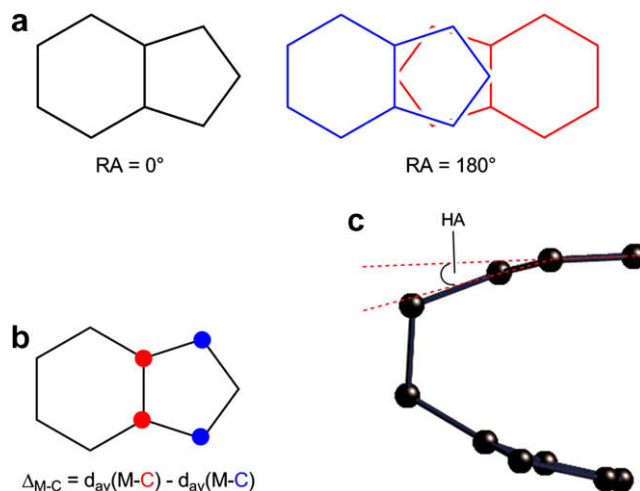


Fig. 8. (a) Rotation angle (RA) of indenyl ligand systems, showing fully eclipsed and fully staggered arrangements of the rings. (b) Calculation of the value of the slip parameter, $\Delta_{\text{M-C}}$. (c) Side view of *rac-2* with Co atom, methyl groups and the upper aryl ring removed for clarity, showing the hinge angle (HA) formed on the lowering of the *ipso*-carbon out of the plane of the five-membered ring.

Table 4
Structural parameters of neutral and oxidised cobalt-containing EBI^* species

Compound	RA (°)	$\Delta_{\text{M-C}}$	HA (°)
<i>rac-2</i>	148.6	0.145	11.0
<i>rac-5</i> · CH_2Cl_2	148.4/140.9	0.057	7.7
<i>meso-5</i>	17.5	0.071	7.6

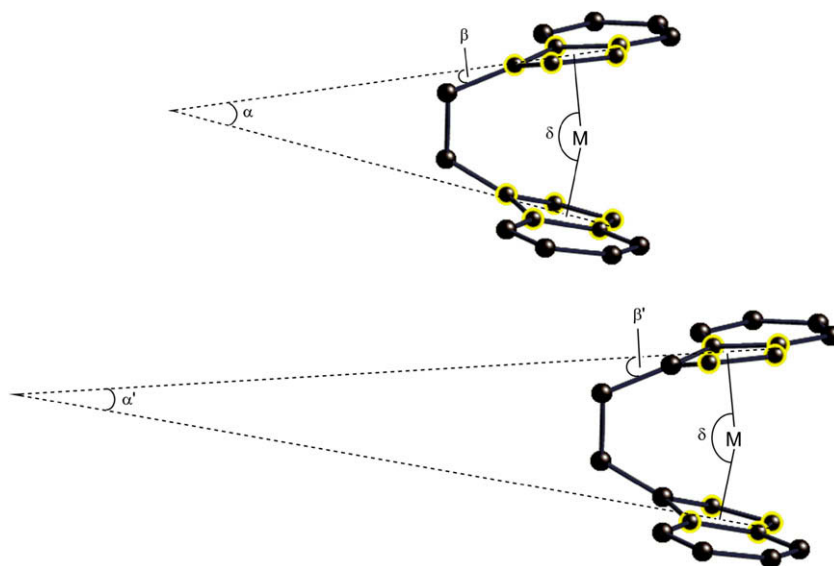


Fig. 9. Representation of the geometric parameters listed in Table 5; α and β are formed as for cyclopentadienyl species from the best plane of the five membered ring, α' and β' apply in the case of EBI in which the *ipso*-carbon lies out of the plane of the other four carbon atoms of the five-membered ring.

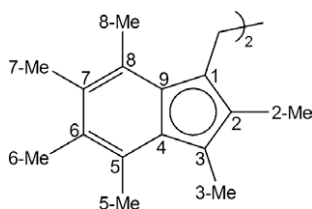


Fig. 10. Numbering scheme for the ^1H and ^{13}C NMR assignment of *rac* and *meso*-4.

3. Experimental details

3.1. General comments

All manipulations were performed under an atmosphere of N_2 using standard Schlenk line techniques or a MBraun UNIlab glove-box, unless stated otherwise. Solvents used were dried by reflux over sodium-benzophenone diketyl (THF) or passage through activated alumina (pentane, hexane, Et_2O) using a MBraun SPS-800 solvent system and thoroughly degassed by passage of a stream of N_2 gas. C_6D_6 was freeze-pump-thaw degassed and dried over a K mirror and d_5 -pyridine was dried by reflux over calcium hydride and purified by trap-to-trap distillation.

^1H and ^{13}C spectroscopy was performed using; a Bruker AVIII 700 with inverse TCI cryoprobe, Bruker AVII 500 with ^{13}C cryoprobe, Varian Unity Plus 500 MHz, Varian Mercury VX-Works 300 MHz or Varian Venus 300 MHz spectrometer and recorded at 300 K. Mass spectrometry used a Bruker MicroTOF spectrometer for ESI or Bruker FT-ICR-MS Apex III spectrometer for EI measurements.

Crystals were mounted on a glass fibre with perfluoropolyether oil and cooled rapidly to 150 K in a stream of N_2 using an Oxford Cryosystems Cryostream unit. Diffraction data were measured using an Enraf-Nonius KappaCCD diffractometer (graphite-monochromated Mo $\text{K}\alpha$ radiation, $\lambda = 0.71073 \text{ \AA}$). Intensity data were processed using the DENZO-SMN package. The structure was then solved using the direct-methods program SIR92, which located all non-hydrogen atoms. Subsequent full-matrix least-squares refinement was carried out using the CRYSTALS program suite [14–16].

Solid-state magnetic susceptibility data were obtained using a Quantum Design MPMS-5 SQUID magnetometer. An accurately weighed sample (0.013 g) was placed into a gelatine capsule and

then loaded into a non-magnetic plastic straw, before being lowered into the cryostat. The field independence of the measurement was verified by measuring the susceptibility as a function of field between -5 and 5 T . Data were then collected employing a field of 0.1 T and finally corrected for the inherent diamagnetism of the sample by use of Pascal's constants [17].

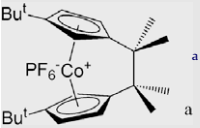
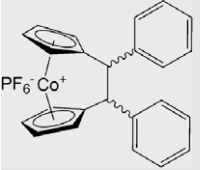
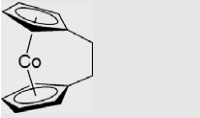
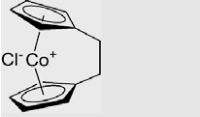
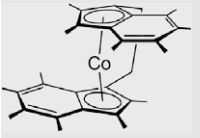
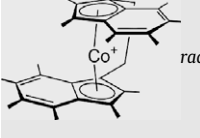
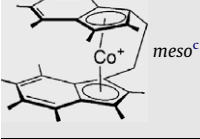
Elemental microanalyses were conducted by Stephen Boyer at London Metropolitan University.

Electrochemical experiments were performed in dry THF containing 0.1 mol L^{-1} $[\text{NBu}^n_4][\text{PF}_6]$ as supporting electrolyte using an Autolab PGStat 20 computer controlled potentiostat (EcoChemie, Utrecht, The Netherlands). Cyclic voltammetric experiments were performed using a three-electrode configuration with a Pt macrodisc electrode (99.99% Goodfellow, UK, area $1.4 \pm 0.2 \times 10^{-3} \text{ cm}^2$) as the working electrode, a Pt gauze as the counter electrode and a Ag wire as the pseudo-reference electrode. The Ag wire pseudo-reference electrode was calibrated to the ferrocene/ferrocenium couple in THF, relative to which all standard potentials are reported. A scan rate of 100 mV s^{-1} was used and measurements were performed under an inert N_2 atmosphere. The Pt working electrodes were polished using alumina slurries of decreasing particle size (1.0 – $0.3 \text{ }\mu\text{m}$, Buehler, USA). After each successive polishing the electrodes were briefly sonicated in ethanol to remove any adhered microparticles, and allowed to thoroughly dry before immersion in the dry THF electrolyte under a N_2 atmosphere.

3.2. Synthesis of $\{(\text{C}_9\text{Me}_6)_2\text{C}_2\text{H}_4\}\text{Na}_2$, EBI* Na_2 (**1**)

BrCN (2.89 g , $2.72 \times 10^{-3} \text{ mol}$) was added under a N_2 flush to a $-78 \text{ }^\circ\text{C}$ slurry in Et_2O of Ind^*Li (6.00 g , $2.72 \times 10^{-3} \text{ mol}$), prepared by literature procedure [18]. The reaction mixture was stirred at $-78 \text{ }^\circ\text{C}$ for 2 h then allowed to warm to room temperature, upon which the off-white precipitate dissolved to give a yellow solution. After stirring for 15 h under a dynamic pressure of N_2 to allow venting of HCN produced, volatiles were removed under vacuum. Extraction with $30 \text{ }^\circ\text{C}$ pentane and passing the resulting solution through silica afforded 2,3,4,5,6,7-hexamethyl-1-methylene-indene, $\text{C}_{16}\text{H}_{20}$ as a bright yellow solid. Yield: 4.10 g , 71% . ^1H NMR (300 MHz) (C_6D_6) δ (ppm): 1.91, 2.08 (both s, 3H, Me), 2.11 (s, 6H, Me), 2.30, 2.36 (both s, 3H, Me), 5.56, 5.84 (both s, 1H, CH_2). ^{13}C NMR (300 MHz) (C_6D_6) δ (ppm): 9.56, 15.53, 15.91, 16.03,

Table 5
Structural parameters for neutral and cationic ethylidene bridged Co species, as defined in Fig. 9

Compound	α, α' ($^\circ$)	β, β' ($^\circ$)	δ ($^\circ$)	M–C _{pcentroid} (Å)	Ref.
	24.8	9.2	162.1	2.630	[12]
	22.9	12.1/12.3	163.1	1.627	[13]
	27.1	16.6/16.7	158.0	1.717/1.714	[6]
	21.4	12.6/12.3	164.0	1.619/1.615	[6]
	21.0, 14.9	14.7/14.0, 18.3/15.7	165.0	1.704	This work
	17.8, 13.5	19.2/15.8, 19.8/19.2	166.9/167.0	1.638/1.624	This work
	17.2, 13.0	17.5/14.7, 20.3/17.7	167.7	1.633/1.640	This work

^aOne ^tBu group is disordered.

^bIsolated as (EBI⁺Co)₂[CoCl₄](CH₂Cl₂)₂.

^cIsolated as (EBI⁺Co)₂[CoCl₄].CH₂Cl₂.

16.43, 16.64 (Me), 28.84 (CH₂), 126.35, 129.45, 131.49, 131.61, 132.61, 132.22, 134.90, 137.18, 140.37, 150.48 (ring Cs). HRMS (EI): Calc: 212.1565. Found: 212.1567.

Na (0.17 g, 7.56 × 10⁻³ mol) was stirred in THF with naphthalene (1.04 g, 8.11 × 10⁻³ mol) for 15 h, resulting in a deep green solution of C₁₀H₈Na. After cooling to -78 °C, a solution in THF of 2,3,4,5,6,7-hexamethyl-1-methylene-indene (1.50 g, 7.06 × 10⁻³ mol) was added. The mixture was stirred for 2 h at -78 °C and then allowed to warm to room temperature. Removal of the solvent under vacuum afforded a light brown solid, which was washed with Et₂O and filtered to give a light brown pyrophoric powder. Yield: 1.26 g, 76%. ¹H NMR (300 MHz) (d₅-pyridine) δ (ppm): 2.49 (s, 12H, Me), 2.55 (s, 6H, Me), 2.71, 2.72, 3.13 (all s, 6H, Me), 3.94 (s, 4H, C₂H₄). ¹³C NMR (300 MHz) (d₅-pyridine) δ (ppm): 13.59, 16.41, 17.33, 17.46, 18.60, 19.05 (Me), 35.06 (C₂H₄), 97.01, 104.27, 117.68, 118.07, 123.12, 123.17, 123.77, 125.20, 125.79 (ring Cs).

3.3. Synthesis of $\{(C_9Me_6)_2C_2H_4\}Co, EBI^+Co$ (**2**)

Co(acac)₂ (0.14 g, 5.31 × 10⁻⁴ mol) was dissolved in THF, cooled to -78 °C and added to a slurry of **1** (0.25 g, 5.31 × 10⁻⁴ mol) in THF at -78 °C. The reaction mixture was stirred at -78 °C for 15 min then allowed to warm to room temperature under a sealed N₂ atmosphere. After stirring the purple suspension at room temperature for 15 h the solvent was removed under vacuum and the remaining purple solid extracted with 50 °C hexane, giving a purple solution and white residue. The solution was reduced to a minimum volume and cooled to -78 °C to give a purple solid. This solid was filtered, washed twice with -78 °C hexane and dried under vacuum. Single crystals of the *rac*-isomer suitable for X-ray diffraction were obtained via the slow cooling of a hexane solution to -35 °C. Yield: 0.13 g, 51%. ¹H NMR (300 MHz) (C₆D₆) δ (ppm): 14.5 (*b* paramagnetic). HRMS (EI): Calc: 483.2462. Found: 483.2469.

Table 6
Crystallographic data for compounds **2**, *rac-5* · CH₂Cl₂, and *meso-5*

	<i>rac-2</i>	<i>rac-5</i> · CH ₂ Cl ₂	<i>meso-5</i>
Crystal system	Monoclinic	Monoclinic	Monoclinic
Space group	C2/c	P2 ₁	C2/c
<i>a</i> (Å)	23.0232(5)	10.84450(10)	20.6972(3)
<i>b</i> (Å)	9.1871(3)	19.9498(3)	28.2902(6)
<i>c</i> (Å)	13.9675(4)	14.3869(2)	11.1217(2)
α (°)	90	90	90
β (°)	123.4726(14)	94.8344(10)	117.5994(10)
γ (°)	90	90	90
Cell volume (Å ³)	2464.37(13)	3101.47(7)	5771.05(19)
<i>Z</i>	4	2	8
Reflections measured	9559	35468	30285
Unique reflections	2945	13771	6553
<i>R</i> _{int}	0.036	0.044	0.055
Observed reflections (<i>I</i> > 2σ(<i>I</i>))	2275	13753	5923
Parameters refined	210	695	337
Goodness of fit	1.0511	0.9781	1.0000
<i>R</i> ₁	0.0398	0.0405	0.0411
<i>wR</i> ₂	0.0469	0.0777	0.0886

ESDs are given in parentheses.

Anal. Calc. for C₃₂H₄₀Co: C, 79.48; H, 8.34. Found: C, 79.54; H, 8.23%. Crystallographic data are given in Table 6.

3.4. Synthesis of [((C₉Me₆)₂C₂H₄)Co]Cl, [EBI*Co]Cl (**3**)

Compound **2** (0.030 g, 6.20 × 10⁻⁵ mol) was suspended in H₂O, NH₄Cl (0.074 g, 1.24 × 10⁻³ mol) added and the mixture stirred for 15 h in the presence of atmospheric oxygen. The resulting orange suspension was filtered and the solvent removed under vacuum. Extraction with CH₂Cl₂ and removal of the solvent under vacuum afforded an orange residue. Yield: 0.026 g, 81%.

rac-3: ¹H NMR (300 MHz) (CD₂Cl₂) δ (ppm): 1.30, 1.47, 2.38, 2.40, 2.43, 2.78 (all s, 6H, Me), 3.49–3.67, 3.78–3.94 (m, 4H, C₂H₄). ¹³C NMR (300 MHz) (CD₂Cl₂) δ (ppm): 7.61, 10.93, 17.50, 17.69, 17.95, 18.60 (Me), 35.22 (C₂H₄), 84.38, 92.41, 96.43, 100.39, 103.19 (Cs of five-membered ring), 125.02, 130.76, 137.76, 144.13 (Cs at back of six-membered ring). HRMS (ESI): Calc: 483.2457. Found: 483.2451.

meso-3: ¹H NMR (300 MHz) (CD₂Cl₂) δ (ppm): 2.01, 2.06, 2.15 (all s, 6H, Me), 2.18 (s, 12H, Me), 2.40 (s, 6H, Me), 3.53–3.73 (m, 4H, C₂H₄). ¹³C NMR (300 MHz) (CD₂Cl₂) δ (ppm): 10.97, 12.75, 16.74, 17.13, 18.08, 18.13 (Me), 34.47 (C₂H₄), 85.91, 90.83, 93.96, 102.59, 110.28 (Cs of five-membered ring), 123.05, 127.17, 136.23, 140.43 (Cs at back of six-membered ring).

Crystals of the *rac*-isomer suitable for X-ray diffraction were obtained as [*rac*-EBI*Co]₂[CoCl₄] (CH₂Cl₂)₂ (*rac-5* · CH₂Cl₂) by the slow diffusion of Et₂O into a concentrated CH₂Cl₂ solution of isomerically pure *rac-3*. Similarly, single crystals of the *meso*-isomer were obtained as [*meso*-EBI Co]₂[CoCl₄] CH₂Cl₂ (*meso-5*) by the slow diffusion of Et₂O into a concentrated CH₂Cl₂ solution of a 1:1 *rac/meso* mixture of **3**. The indenyl moieties in *rac-5* · CH₂Cl₂ exhibit a considerable degree of liberation. Attempts to model this proved to be laborious and unstable, adding little to the model. Since the disorder does not affect the understanding of the chemistry and the connectivity, the refinement was left with prolate ellipsoids which describe the dynamics very clearly. Crystallographic data are given in Table 6.

rac-5 · CH₂Cl₂: ¹H NMR (300 MHz) (CD₂Cl₂) δ (ppm): 1.17, 1.40 (both bs, 6H, Me), 2.35 (bs, 12H, Me), 2.39, 2.66 (both bs, 6H, Me), 3.24–3.50, 3.54–3.78 (bm, 4H, C₂H₄). CH₂Cl₂ either removed under vacuum drying of sample or overlying the residual CD₂Cl₂ protio peak.

meso-5: ¹H NMR (300 MHz) (CD₂Cl₂) δ (ppm): 1.30, 1.96 (both bs, 6H, Me), 1.99 (bs, 12H, Me), 2.10, 2.31 (both bs, 6H, Me),

3.30–3.48 (bm, 4H, C₂H₄). CH₂Cl₂ either removed under vacuum drying of sample or overlying the residual CD₂Cl₂ protio peak.

3.5. Synthesis of [((C₉Me₆)₂C₂H₄)Co]PF₆, [EBI*Co]PF₆ (**4**)

Compound **2** (0.030 g, 6.20 × 10⁻⁵ mol) was suspended in H₂O, NH₄Cl added and stirred for 15 h in the presence of atmospheric oxygen. The resulting orange suspension was filtered and a saturated solution of NH₄PF₆ added dropwise, resulting in an immediate red-orange precipitate. This precipitate was filtered, extracted with CH₂Cl₂ and evaporated to dryness. Yield: 0.031 g, 79%.

rac-4: ¹H NMR (500 MHz) (CD₂Cl₂) δ (ppm): 1.31 (s, 6H, 2-Me), 1.48 (s, 6H, 3-Me), 2.38 (s, 6H, 6-Me), 2.41 (s, 6H, 5-Me), 2.43 (s, 6H, 7-Me), 2.80 (s, 6H, 8-Me), 3.63 (m, 2H, H_{B,B'}), 3.91 (m, 2H, H_{A,A'}), ²J_{AB} = -15.72 Hz, ³J_{AA'}} = 1.80 Hz, ³J_{A'B}} = 8.00 Hz, ³J_{BB'}} = 11.09 Hz). ¹³C NMR (500 MHz) (CD₂Cl₂) δ (ppm): 6.56 (2-Me), 10.17 (3-Me), 16.90 (6-Me), 16.94 (8-Me), 17.09 (5-Me), 17.96 (7-Me), 34.59 (C₂H₄), 84.79 (3-C), 92.94 (4-C), 96.89 (1-C), 101.00 (9-C), 103.81 (2-C), 125.88 (8-C), 131.80 (5-C), 138.89 (6-C), 145.35 (7-C).

meso-4: ¹H NMR (500 MHz) (CD₂Cl₂) δ (ppm): 2.01 (s, 6H, 6-Me), 2.07 (s, 6H, 5-Me), 2.15 (s, 6H, 7-Me), 2.22 (s, 6H, 3-Me), 2.28 (s, 6H, 2-Me), 2.42 (s, 6H, 8-Me), 3.66 (m, 2H, H_{B,B'}), 3.73 (m, 2H, H_{A,A'}), ²J_{AB} = -15.66 Hz, ³J_{AA'}} = 7.71 Hz, ³J_{A'B}} = 6.35 Hz, ³J_{BB'}} = 8.10 Hz). ¹³C NMR (500 MHz) (CD₂Cl₂) δ (ppm): 9.43 (2-Me), 11.56 (3-Me), 16.11 (5-Me), 16.64 (6-Me), 17.24 (7-Me), 17.49 (8-Me), 33.48 (C₂H₄), 86.40 (3-C), 91.43 (4-C), 94.35 (1-C), 103.15 (2-C), 104.18 (9-C), 123.97 (8-C), 128.23 (5-C), 137.51 (6-C), 141.78 (7-C).

4. Conclusions

The new ligand ethylene-bis-hexamethylindenyl (EBI*), ((C₉Me₆)₂C₂H₄)²⁻ has been synthesised and used to prepare *ansa*-bis-indenylcobaltocenes in good yield. Not only are these very rare examples of strained cobaltocenes, they are the first examples of a hydrocarbon-bridged cobaltocenophane containing peralkylated ring systems.

Supplementary material

CCDC 695516, 695517, 695518 contain the supplementary crystallographic data for compounds **2**, *meso-5* and *rac-5* · CH₂Cl₂, respectively. These data can be obtained free of charge from The Cambridge Crystallographic Data Centre via www.ccdc.cam.ac.uk/data_request/cif.

Acknowledgements

The authors thank Dr. Nicholas Rees for assistance with the NMR assignment of **4**, and the EPSRC for financial support.

References

- [1] P.J. Shapiro, Coord. Chem. Rev. 231 (2002) 67–81.
- [2] B. Wang, Coord. Chem. Rev. 250 (2006) 242–258.
- [3] J.M. Nelson, P. Nguyen, R. Petersen, H. Rengel, P.M. Macdonald, A.J. Lough, I. Manners, N.P. Raju, J.E. Greedan, S. Barlow, D. O'Hare, Chem. Eur. J. 3 (1997) 573–584.
- [4] D.E. Herbert, U.F.J. Mayer, I. Manners, Angew. Chem., Int. Ed. 46 (2007) 5060–5081.
- [5] S.C. Jones, S. Barlow, D. O'Hare, Chem. Eur. J. 11 (2005) 4473–4481.
- [6] U.F.J. Mayer, J.P.H. Charmant, J. Rae, I. Manners, Organometallics 27 (2008) 1524–1533.
- [7] M. Rieckhoff, U. Pieper, D. Stalke, F.T. Edelman, Angew. Chem., Int. Ed. Engl. 32 (1993) 1079–1081.
- [8] M. Tacke, S. Fox, L. Cuffe, J.P. Dunne, F. Hartl, T. Mahabiersing, J. Mol. Struct. 559 (2001) 331–339.
- [9] M. Herberhold, Y.-X. Cheng, G.-X. Jin, W. Milius, Z. Naturforsch., B: Chem. Sci. 55 (2000) 814–820.

- [10] H. Werner, G. Mattmann, A. Salzer, T. Winkler, *J. Organomet. Chem.* 25 (1970) 461–474.
- [11] S.A. Westcott, A.K. Kakkar, G. Stringer, N.J. Taylor, T.B. Marder, *J. Organomet. Chem.* 394 (1990) 777–794.
- [12] M.J. Drewitt, S. Barlow, D. O'Hare, J.M. Nelson, P. Nguyen, I. Manners, *Chem. Commun.* (1996) 2153–2154.
- [13] S. Fox, J.P. Dunne, M. Tacke, D. Schmitz, R. Dronskowski, *Eur. J. Inorg. Chem.* (2002) 3039–3046.
- [14] A. Altomare, G. Cascarano, C. Giacovazzo, A. Guagliardi, M.C. Burla, G. Polidori, M. Camalli, *J. Appl. Crystallogr.* 27 (1994) 435.
- [15] P.W. Betteridge, J.R. Carruthers, R.I. Cooper, K. Prout, D.J. Watkin, *J. Appl. Crystallogr.* 36 (2003) 1487.
- [16] Z. Otwinowski, W. Minor, *Methods Enzymol.* 276 (1997) 307.
- [17] C.J. O'Connor, *Prog. Inorg. Chem.* 29 (1982) 203–283.
- [18] D. O'Hare, J.C. Green, T. Marder, S. Collins, G. Stringer, A.K. Kakkar, N. Kaltsoyannis, A. Kuhn, R. Lewis, et al., *Organometallics* 11 (1992) 48–55.